

Growth mode in Si(100)-(2×1) epitaxy by low-temperature chemical-vapor deposition

Peng-Hung Wu and Deng-Sung Lin*

Institute of Physics, National Chiao-Tung University, 75 Bo-Ai Street, Hsinchu, Taiwan

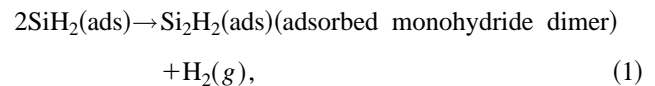
(Received 29 December 1997)

This study investigates the growth processes of Si on Si(100)-(2×1) during ultrahigh vacuum chemical vapor deposition using disilane as the source gas. The evolution of surface morphology and atomic ordering during growth at temperatures between 300 and 600 °C is examined in real time by high-temperature scanning tunneling microscopy. Directly imaging various growth kinetic processes, such as pure step-flow growth, double step-flow growth, two-dimensional nucleation growth, and surface passivation at different substrate temperature ranges clearly illustrates the growth mechanisms for the model chemical vapor deposition growth system and provides interesting comparison with results of Monte Carlo simulations and those of solid phase molecular-beam epitaxy. [S0163-1829(98)05619-7]

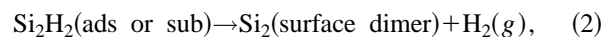
I. INTRODUCTION

In recent years, increasing emphasis has been placed on surface atomistic processes and growth mechanisms during low-temperature ultrahigh vacuum chemical vapor deposition (UHV-CVD) of group IV elements.¹⁻¹⁴ Among those growth systems, Si(100) homoepitaxy using disilane has been most extensively studied as a model system owing to its importance in both fundamental science and industrial applications.¹⁻¹¹ Compared with other conventional gas sources such as SiH₄ and SiH₂Cl₂, disilane (Si₂H₆) offers a higher sticking probability on Si and Ge surfaces and lower decomposition activation energy for both gas phases and surface reactions, thereby allowing a lower deposition temperature.^{1,2,12} The Si(100) surface typically exhibits a two-domain (2×1) dimer structure with a dangling bond for each surface atom.

Upon adsorption above 120 K on the Si(100)-(2×1) surface, a Si₂H₆ molecule undergoes dissociative chemisorption by cleaving the relatively weaker Si-Si bond to form two SiH₃ (trihydride) radicals on dangling-bond sites.^{4,8} A SiH₃ radical becomes unstable at higher temperatures and further decomposes into a SiH₂ (dihydride) species and a H atom, which subsequently reacts with a nearby dangling bond to form SiH (monohydride). At room temperature (RT), disilane exposure of Si(100) results primarily in the presence of SiH₂ and SiH radicals on the surface. SiH₂ species further decomposes into monohydride (SiH) and two SiH radical pairs to form a monohydride dimer (Si₂H₂) at 200–350 °C. At higher temperatures, the desorption of hydrogen from the monohydride dimers takes place and epitaxial Si atoms are left on the surface. Correspondingly, the Si(100) surface under disilane exposure can exhibit a mixture of Si dangling bonds and monohydride, dihydride, and trihydride species, depending on the experimental conditions.^{4,6,7,11} Interestingly, the H₂ temperature-programmed desorption spectra on the RT disilane-saturated Si(100) surface markedly resembles that of H-saturated Si(100).¹⁵ Two desorption maxima, β₁ and β₂, appear at 525 and 410 °C, respectively. As generally accepted, the β₂ and β₁ desorption states occur upon the following reactions:



and



respectively.⁴ In Eqs. (1) and (2), (ads), (sub), and (g) denote an adsorbed species, species formed on the substrate, and desorbed gas molecular, respectively. Notably, the H atoms on the adsorbed monohydride dimers [Si₂H₂(ads)] can migrate to the substrate surface and form substrate monohydride dimers [Si₂H₂(sub)]. Therefore, the H₂ molecules can desorb from either the adsorbed or substrate monohydride dimers as indicated in Eq. (2).

In this work, we report on various growth kinetic processes of Si/Si(100)-(2×1) during low-temperature UHV-CVD from Si₂H₆. The atomistics of Si solid phase molecular-beam epitaxy (MBE) have been extensively studied.¹⁶⁻¹⁸ Upon MBE Si deposition on Si(100) in the temperature range of 300–500 °C, two-dimensional (2D) islands nucleate on the terrace, grow, and coalesce to form a new layer. At higher temperatures, adatoms are highly mobile on the terrace and adhere to steps, leading to the step-flow growth. Previous investigations have examined the same Si/Si(100) CVD growth system by reflection high-energy diffraction (RHEED),^{1,9} reflectance anisotropy (RA),⁹ and STM using the conventional “growth interruption-observation” method.⁴⁻⁷ By simultaneously measuring RA and RHEED, Zhang *et al.* identified the step-flow growth mode above 650 °C and the 2D nucleation growth mode between 550 and 650 °C.⁹ Using STM, Lin *et al.* observed denuded zones and the island coarsening phenomena;⁶ Bronikowski, Wang, and Hamers demonstrated that the antiphase boundaries act as nucleation centers during low-temperature epitaxy.⁵ According to Boland, multilayer growth occurs on the surface, which remains largely H passivated.⁷ In addition, Mizushima *et al.* performed Monte Carlo simulations, indicating that the surface hydrogen atoms preferentially attach to step edges and block the growth front.¹⁰ This study employs high-temperature scanning tunneling microscope (VT-STM) to observe in real time the evolution of surface mor-

phology during Si CVD in atomic resolution and, therefore, provides an extremely comprehensive understanding of the growth features over the most interesting temperature range (300–600 °C), in which hydrogen influences the growth kinetics. Our results are also compared with recent results of Monte Carlo simulations and those from the corresponding MBE.

II. EXPERIMENTAL PROCEDURE

STM measurements were taken in a stainless-steel chamber equipped with a bolt-on commercial VT-STM system (Omicron). The chamber has a base pressure of 1×10^{-10} Torr. The tips of the STM were electrochemically etched tungsten wires. All images were obtained in a constant current mode with a tunneling current of ~ 0.3 nA and a tip bias of 2.0 V. An image is typically acquired in 120–300 s, depending on the scanning size and surface roughness. The figures presented in this paper show selected frames out of the image sequences taken continuously during the growth. Slight distortions due to thermal drift were not adjusted.

The Si(100) samples were sliced from boron-doped wafers with an electrical resistivity of around $10 \Omega \text{ cm}$, corresponding to a dopant concentration of approximately $1.5 \times 10^{15} \text{ cm}^{-3}$. The wafer's misalignment is around 0.1° toward $\langle 011 \rangle$. Substrate cleaning involved outgassing at $\sim 900 \text{ K}$ for 10 h, followed by dc heating to $\sim 1450 \text{ K}$ for a few seconds. Disilane (Voltaix, ultrahigh purity grade) was introduced into the chamber through a precision leak valve. Next, the dosing pressure [$(1-2) \times 10^{-8}$ Torr] was monitored by an ionization gauge that did not directly face the sample. The pressure readings of the ion gauge were calibrated by the gauge's sensitivity to Si_2H_6 , which is around 2.4 relative to air.¹² The sample was annealed by passing a current through it. Its temperature was measured with an infrared pyrometer using a Ge diode and calibrated by a thermal couple attached to a dummy sample.

III. RESULTS AND DISCUSSION

A. Step-flow growth at $T=600^\circ\text{C}$

Figure 1(a) depicts a $5000 \times 2500\text{-}\text{\AA}^2$ STM image of the initially clean Si(100)-(2 \times 1) surface after the sample is heated and maintained at 600°C for about 30 min. At this scale, individual atoms and dimers cannot be viewed. The primary features in Fig. 1(a) denote alternatively smoother and rougher steps (so-called S_A and S_B , respectively). Each step separates two degenerate reconstruction terraces (T_A and T_B) with their dimer rows running parallel (perpendicular) to the domain edges. At this temperature, the step edges appear hairy due to thermal-induced fluctuations.

Figures 1(b)–1(e) illustrate the UHV-CVD homoepitaxial growth experiment at 600°C . In this study, the surface of Fig. 1(a) is exposed to disilane ($\sim 2 \times 10^{-8}$ Torr) for 11.2, 27.2, 38, 100 L (1 L = 10^{-6} Torr s) for Figs. 1(b)–1(e), respectively. Prior to the gas exposure, an area with three-dimensional (3D) clusters appearing at the upper right corner in Figs. 1(b) and 1(c) is located for the experiment. The clusters are used as a marker and the largest 3D island measures $\sim 9 \text{ \AA}$ in height. As the exposure increases, the 3D

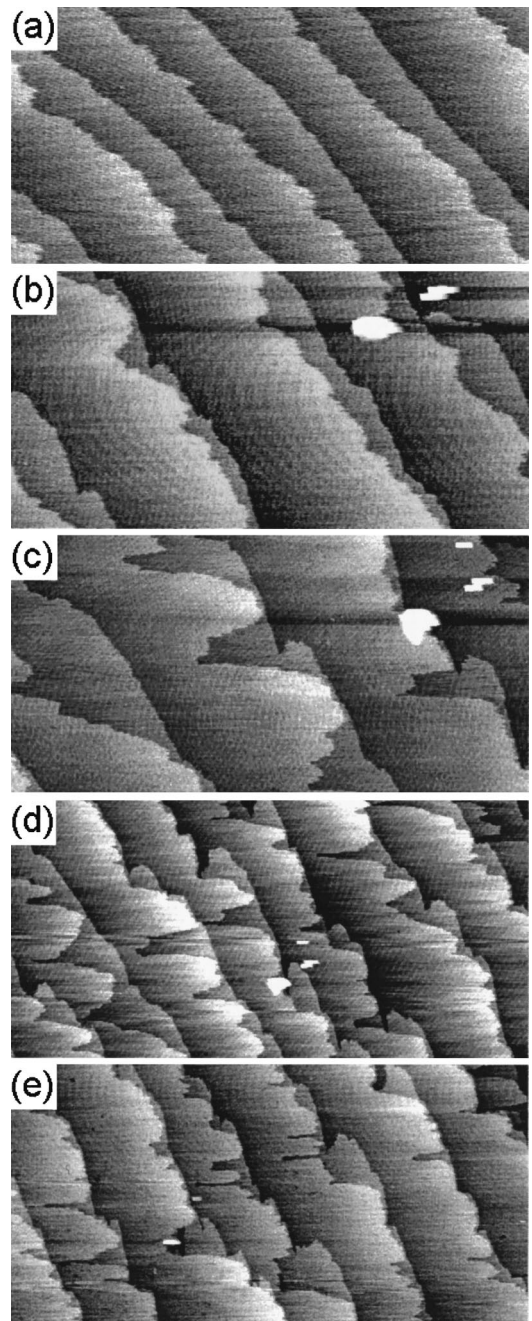


FIG. 1. Real-time STM images of a growth sequence of Si on Si(100)-(2 \times 1) at 600°C . Images (a)–(e) show the surfaces after disilane exposure of 0, 11.2, 27.2, 38.6, and 100 L, respectively. The images are of size $5000 \times 2500 \text{ \AA}^2$ for (a)–(c) and $10\,000 \times 5000 \text{ \AA}^2$ for (d), (e).

clusters are gradually buried by the grown film. After 100 L of disilane exposure, only a small bump less than 1 \AA in height can still be found in Fig. 1(e), indicating that a film of $\sim 6 \text{ ML}$ thick is grown. By aligning the markers in two consecutive images, the total thickness of the grown film, its components due to the advance of S_B and S_A steps, and the evolution of the fractional coverage (Θ_B) of T_B domains for various disilane exposure are deduced and plotted in Fig. 2(a). According to the slope of the growth curve for the total thickness in Fig. 2(a), the initial growth rate is approximately $\sim 0.055 \text{ ML/L}$. The reactive sticking probability of disilane is therefore around 0.05, which closely corresponds to that

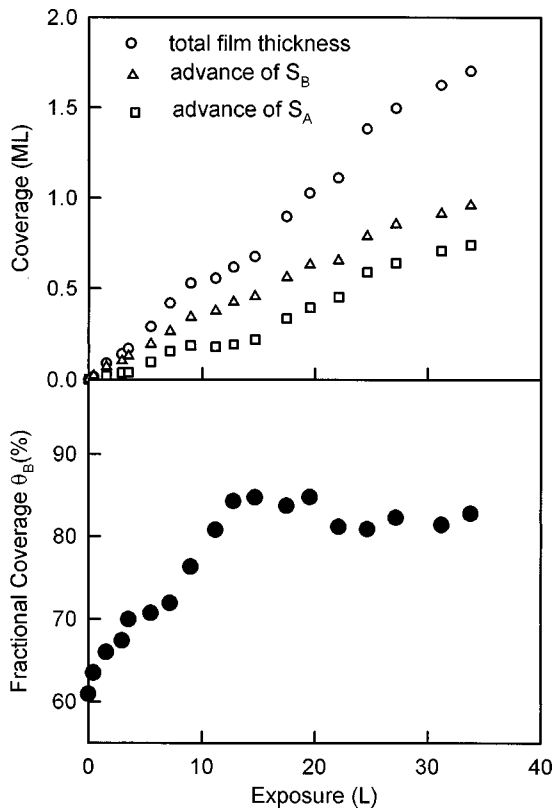


FIG. 2. (a) Total thickness of the grown film and its components due to the advance of S_B and S_A steps and (b) evolution of the fractional coverage θ_B for various disilane exposure at 600 °C.

deduced from a time-of-flight direct recoiling measurement.³ Since the tip shades the scanning area, the actual exposure (depending on the radius of tips and the scanning size) is reduced. The reduction of exposure should be within a small percentage for a scan range of $5000 \times 5000 \text{ \AA}^2$ and a typical tip radius of less than 1000 \AA .¹⁹ However, growth rates up to a factor of 2 smaller are occasionally observed with some tips, indicating the STM tips occasionally have a large radius. At this temperature, H desorbs upon adsorption of disilane and, hence, the surface coverage of H is nearly zero since its desorption temperature (the so-called β_1 state, $\sim 525 \text{ °C}$) is well below the growth temperature. The adsorbed Si adatoms left behind after H desorption are sufficiently mobile to reach the step edges, leading to step-flow growth. The S_B steps appear to advance faster, leading to the formation of a nearly single-domain surface, as Fig. 1(b) depicts. As the disilane dosage increases, the growth proceeds by a double-step flow and the surface remains nearly single domain as revealed in Figs. 1(d) and 1(e). Quantitatively, the slopes of the growth curves in Fig. 2(a) indicate that the advance of S_B steps is nearly three times faster than that of S_A steps in the initial stage. This can be attributed to the fact that the adatom incorporation rate into S_B steps is markedly higher than that of S_A steps, as concluded by several previous studies.^{16,17} The surface prior to the growth [Fig. 1(a)] consists of alternating T_A and T_B domains. The initial amount of θ_B is about 60%. As growth continues, θ_B increases to $\sim 85\%$ after growing less than 1 ML and, then, remains largely at the same value, as Fig. 2(b) depicts. Similar to that found in the growth by MBE,¹⁶ θ_B never reaches

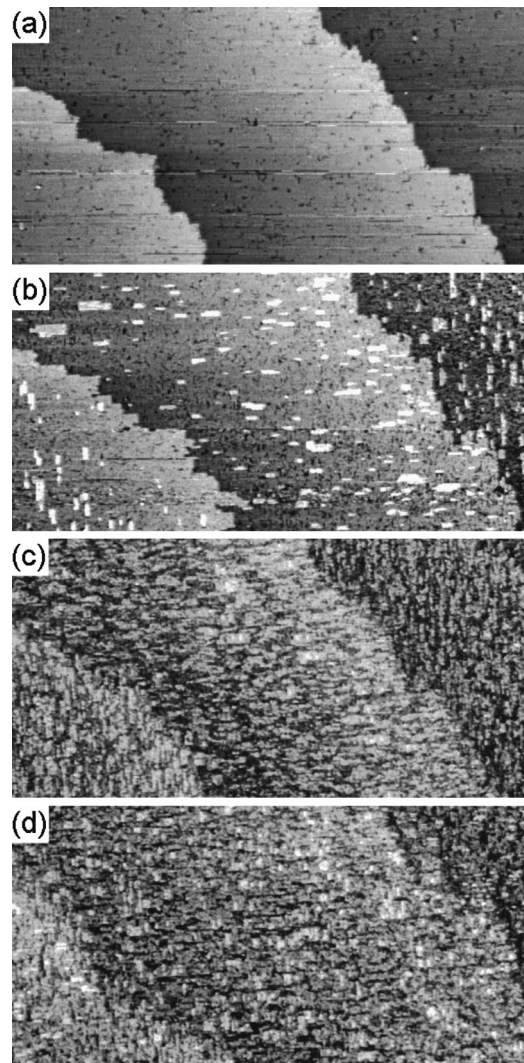


FIG. 3. STM images ($2000 \times 1000 \text{ \AA}^2$) of a growth sequence of Si on Si(100)-(2×1) at 440 °C. Images (a)–(d) are recorded at a disilane exposure of 0, 2.5, 20, and 50 L, respectively.

100% due to step pinning at defects, causing cusps on the S_B steps in Figs. 1(c)–1(e). Overall, the step-flow growth behavior resembles that observed during MBE, indicating that hydrogen, which has an extremely short surface lifetime at this temperature, only slightly influences the growth.

B. Two-dimensional nucleation growth at $T=440\text{--}490 \text{ °C}$

Figure 3 displays the selected STM images of the Si(100) surface during exposure to disilane while maintaining at 440 °C, a temperature between the β_1 and β_2 desorption peaks in TPD. The initially clean Si(100)-(2×1) surface [Fig. 3(a)] has a low concentration of DV's, which appear as dark spots. After exposing to disilane for 2.5 L, the surface shows that small two-dimensional (2D) islands nucleate and grow as revealed in Fig. 3(b). The 2D islands are clean epitaxial Si islands, as evidenced by the fact that they have the same apparent height with the substrate monoatomic steps. At this temperature, the bimolecular reaction between two surface SiH_2 groups into a Si_2H_2 monohydride dimer and a gas phase H_2 molecule [Eq. (1)] is completed. Although the β_1 desorption peak upon annealing a disilane-saturated sur-

face reaches as high as 525 °C, the H₂ desorption from adsorbed Si₂H₂ monohydride dimers occurs at a slow rate at 410 °C.^{7,10} The H atoms on the adsorbed monohydride dimers can also hop to the available surrounding dangling bonds of substrate dimers, leaving “clean” adsorbed Si dimers to nucleate into 2D islands.⁴ Furthermore, H atoms released from the dissociation of SiH₃ groups bond to clean substrate dimers to form substrate monohydride dimers. Consequently, the substrate Si₂H₂ monohydride dimers accumulate. Figure 3(b) confirms such an accumulation by an increasing concentration of dark spots. Due to the electronic effect, a surface monohydride dimer has a markedly (nearly 1 Å) lower apparent height than an adjacent clean Si dimer in the occupied state.²⁰ Therefore, it appears similar to a missing dimer defect in the images. In Fig. 3(b) the 2D islands have a shape anisotropy of about a factor of 3. The island density is substantially higher than that observed in the Si MBE deposition at the same temperature range.¹⁷ As predicted by the Monte Carlo simulation, this difference in the island density between the solid phase MBE and CVD can be attributed to the substantial increase in the effective activation energy for Si diffusion due to the presence of H on the surface.^{10,21} Figure 3(c) depicts that as the growth proceeds further, the terraces are increasingly covered by an increasing number of 2D islands. However, the islands do not continue to grow in size, indicating that the growth front of the 2D islands is eventually blocked by H atoms on the substrate since the ends of clean epitaxial Si islands are weak adsorption sites for H.⁴ As disilane exposure continues, growth goes on to fill the first layer and starts on the second layer, as Figs. 3(d) and 4(a) reveal. The actual amount of H accumulated on the surface such as that of Fig. 4(a) is difficult to be extracted owing to the inability of resolution in real-time imaging to distinguish monohydride dimers from missing dimer defects. However, the effect of the surface monohydride species can be discerned by comparing Fig. 4(a) and Fig. 4(b), which are taken before and after halting the disilane gas, respectively. The diffusion of Si adatoms accelerates as H atoms on the surface are gradually depleted. Figure 4(b) also reveals that small islands and clusters adhere to step edges or coalesce to form larger islands.

Figures 5(a)–5(d) display the CVD growth sequence at 490 °C, a temperature near the β_1 desorption peak. The evolution of the surface morphology during the growth closely resembles that at 450 °C. However, compared to growth at 450 °C, the 2D epitaxial islands can grow larger in size at 490 °C and the island density is smaller. These observations are expected since higher substrate temperature leads to lower residual surface H concentration and larger effective Si diffusion length. Nevertheless, ideal layer-by-layer growth does not occur. Figure 5(c) indicates that the second layer growth starts before the first layer completes growth. Further growth leads to increased roughness as revealed in Figs. 5(d) and 6. Such growth is ascribed to the fact that antiphase domain boundaries (APB) provide preferred nucleation sites for growth in the next layer.⁵ Since epitaxial islands nucleate randomly, the distance between dimer rows of two neighboring 2D islands on a single-domain terrace can be either odd or even lattice constants. Therefore, islands could have the same (even) or opposite (odd) phases. When two neighboring 2D islands with opposite phases grow and intersect, an

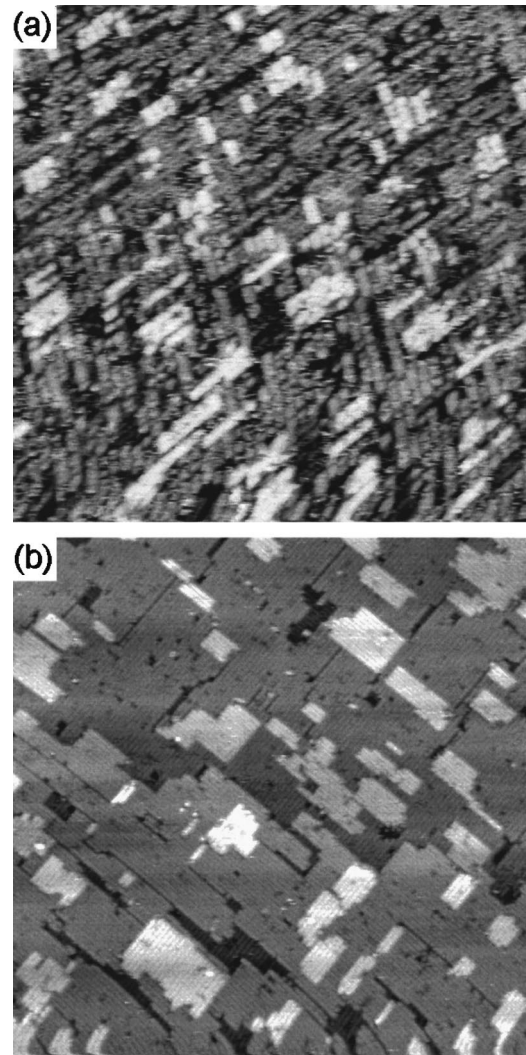


FIG. 4. (a) STM image ($500 \times 500 \text{ \AA}^2$) of the same growth sequence as in Fig. 3 at a disilane exposure of 65 L. (b) The same surface after halting disilane exposure for 20 min. The area is $800 \times 800 \text{ \AA}^2$.

APB arises. At temperatures ranging between 490 and 600 °C, the island nucleation growth and the step-flow growth occur simultaneously, as shown in Fig. 7.

C. $T < 400 \text{ }^\circ\text{C}$

At temperatures well below the β_1 desorption peak, surface dangling bonds are progressively occupied by each of the adsorption fragments including SiH_x hydrides and H; the surface eventually becomes passivated and ultimately prevents multilayer growth. Figures 8(a)–8(c) illustrate the Si(100) surfaces after 30, 60, and 160 L disilane exposure at 370 °C, respectively. In Fig. 8(a), one-dimensional islands orthogonal to the substrate dimer rows are randomly dispersed and cover $\sim 54\%$ of the surface. Bright features occasionally appear in the images, which can be attributed to the bonding of disilane fragments to the new epitaxy layer.⁷ Figures 8(b) and 8(c) indicate that the surface morphology remains largely the same after much more additional exposure. This finding implies that the surface in Fig. 8(a) is largely passivated and that the rate of H₂ desorption from

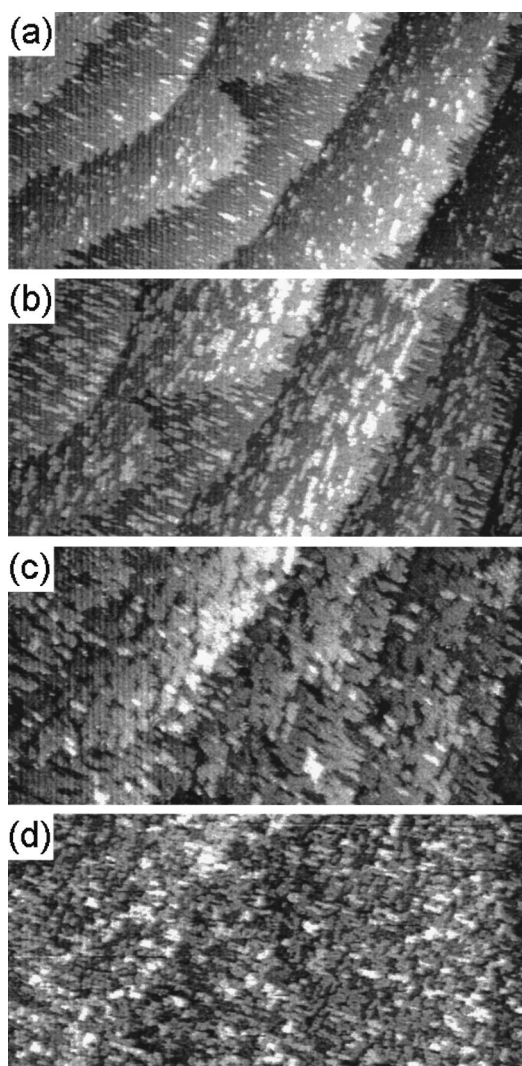


FIG. 5. STM images ($5000 \times 2500 \text{ \AA}^2$) of a growth sequence at $490 \text{ }^\circ\text{C}$. Images (a)–(d) are recorded at a disilane exposure of 1.3, 6, 20, and 48 L, respectively.

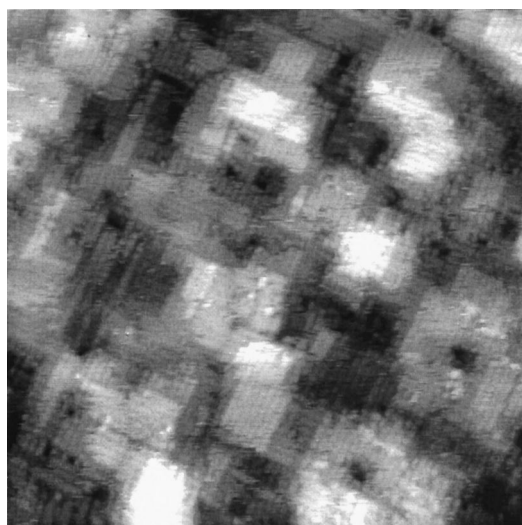


FIG. 6. Small area ($500 \times 500 \text{ \AA}^2$) image of the same growth sequence as in Fig. 5. The disilane exposure is 103 L.

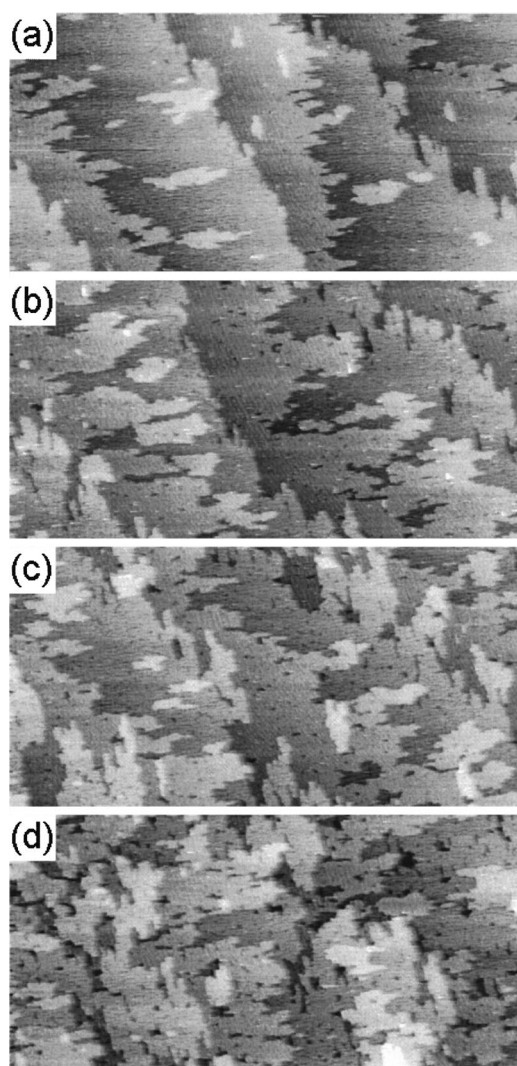


FIG. 7. Real-time STM images of a growth sequence at $530 \text{ }^\circ\text{C}$. The images are of size $6000 \times 3000 \text{ \AA}^2$. Images (a)–(d) show the surfaces after disilane exposure of 5.6, 18, 36, and 98 L, respectively.

this surface is nearly zero. Compared to Fig. 8(a), the coverage of 1D islands and the bright features on the 1D islands in Fig. 8(c) slightly increase, presumably due to the liberation of dangling bonds after gradual H_2 desorption from adsorbed Si_2H_2 dimers. Following continuous growth, the surface such as that in Fig. 8(a) resembles that prepared by $400 \text{ }^\circ\text{C}$ annealing on a room-temperature disilane-saturated surface.⁷ According to Ref. 7, the 1D rows are formed by monohydride dimers. The synchrotron core-level photoemission spectrum for a disilane-saturated Si(100) surface after $400 \text{ }^\circ\text{C}$ annealing also indicates that all surface dangling bonds are saturated by H.¹¹ The above results demonstrate not only that both the 1D islands and the remaining substrate areas in Fig. 8 consist of Si_2H_2 monohydride dimers, but also that the monohydride dimer structure resists multilayer growth at $370 \text{ }^\circ\text{C}$. In Ref. 7, Boland successfully grew epitaxial layers on a (2×1) monohydride surface (prepared by atomic H adsorption) at $415 \text{ }^\circ\text{C}$ followed by a 5-min postanneal at $375 \text{ }^\circ\text{C}$. Boland also found that the new surface retains the (2×1) monohydride structure and, therefore, concluded that epitaxy growth of Si on a monohydride surface occurs at

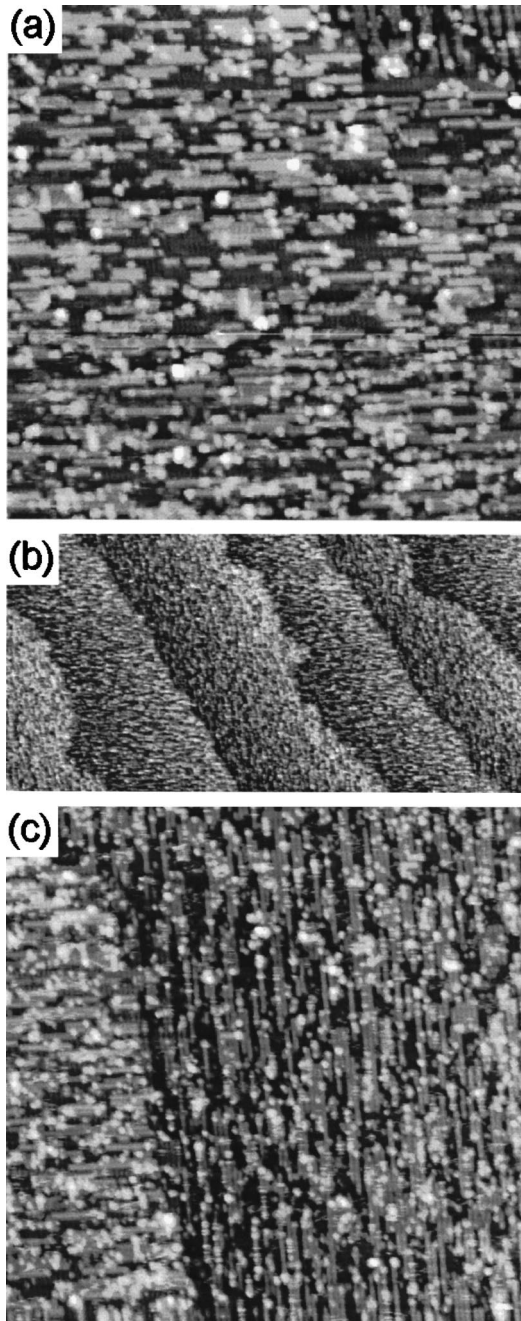


FIG. 8. Real-time STM images of Si(100) dosed by (a) 30, (b) 60, and (c) 160 L of disilane at 370 °C. The images are of size $700 \times 700 \text{ \AA}^2$ for (a), (c) and $4000 \times 2000 \text{ \AA}^2$ for (b).

415 °C in part due to a direct interaction between disilane and the monohydride surface. As discussed above and in Sec. III B, Figs. 3 and 8 imply that the desorption rate of H_2 from a monohydride surface increases sharply from 370 to 440 °C. It is likely that the different growth conditions (growth at a higher temperature followed by postannealing at a lower temperature versus continuous real-time growth) led

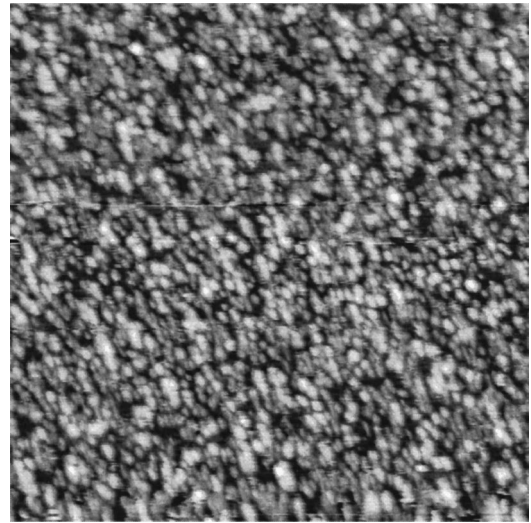


FIG. 9. Real-time STM images ($700 \times 700 \text{ \AA}^2$) of Si(100) saturated with a 15 L disilane at 300 °C.

to the discrepancy between Ref. 7 and this work regarding the degree of interaction between disilane and the monohydride surface.

At 300 °C, a temperature well below the β_2 desorption state, the dissociation of dyhydrides [Eq. (1)] cannot occur and the Si(100)- (2×1) surface is saturated by poorly ordered surface SiH_2 species, as depicted in Fig. 9. Nevertheless, short Si_2H_2 monohydride strings with a local (2×1) structure can be discerned in the image by close inspection.

IV. SUMMARY

This work uses real-time HT-STM to examine the growth of Si on Si(100) during UHV-CVD. Those results provide detailed information regarding the growth speed of different steps, the evolution of the surface ordering and morphology, and the growth modes for various temperatures. At a disilane pressure of around 2×10^{-8} Torr, the growth at $>570 \text{ °C}$ proceeds with a pure step-flow mode during the initial stage. The growth at S_B step is approximately three times faster than S_A . After a single-domain surface is obtained, double-step flow growth occurs. Between 450 and 500 °C, two-dimensional nucleation growth occurs. In addition, various amounts of H atoms are present on the surface, but do not prevent growth. The H atoms reduce the effective diffusion length of Si adatoms, leading to a large island density and ultimately causing an imperfection of layer-by-layer growth. Below approximately 400 °C, the surface is passivated by various hydride species, thereby prohibiting multilayer growth.

ACKNOWLEDGMENTS

The authors would like to thank the National Science Council, Taiwan, for financially supporting this work under Contract No. NSC87-2112-M009-003.

*Electronic address: dslin@cc.nctu.edu.tw

¹W. K. Liu, S. M. Mokler, N. Ohtani, and B. A. Joyce, *Surf. Sci.* **264**, 301 (1992); S. M. Mokler, W. K. Liu, N. Ohtani, J. Zhang,

and B. A. Joyce, *ibid.* **275**, 401 (1992).

²F. Chollet, E. Andre, W. Vandervorst, and M. Caymax, *J. Cryst. Growth* **157**, 168 (1995).

- ³S. M. Gates and S. K. Kulkarni, *Appl. Phys. Lett.* **60**, 53 (1992).
- ⁴Y. Wang, M. J. Bronikowski, and R. J. Hamers, *Surf. Sci.* **311**, 64 (1994).
- ⁵M. J. Bronikowski, Y. Wang, and R. J. Hamers, *Phys. Rev. B* **48**, 12 361 (1993).
- ⁶D.-S. Lin, E. Hirschorn, T.-C. Chiang, R. Tsu, D. Lubben, and J. E. Greene, *Phys. Rev. B* **45**, 3494 (1992).
- ⁷J. J. Boland, *Phys. Rev. B* **44**, 1383 (1991).
- ⁸F. Bozso and Ph. Avouris, *Phys. Rev. B* **38**, 3943 (1988).
- ⁹J. Zhang, A. G. Taylor, A. K. Lees, J. M. Fernandez, B. A. Joyce, D. Raisbeck, N. Shukla, and M. E. Pemble, *Phys. Rev. B* **53**, 10 107 (1996).
- ¹⁰K. Mizushima, D. D. Vvedensky, P. Smilauer, A. Zangwill, J. Zhang, and B. Joyce, *J. Cryst. Growth* **175/176**, 509 (1996).
- ¹¹D.-S. Lin, T. Miller, T.-C. Chiang, R. Tsu, and J. E. Greene, *Phys. Rev. B* **48**, 11 846 (1993).
- ¹²S. M. Gates, *Surf. Sci.* **195**, 307 (1988).
- ¹³I. Goldfard, P. T. Hayden, J. P. Hayden, J. H. G. Owen, and G. A. D. Briggs, *Phys. Rev. Lett.* **78**, 3959 (1997).
- ¹⁴D.-S. Lin, K.-H. Huang, T.-W. Pi, and R.-T. Wu, *Phys. Rev. B* **56**, 4878 (1997); D.-S. Lin, T. Miller, and T.-C. Chiang, *J. Vac. Sci. Technol. A* **15**, 919 (1997).
- ¹⁵C. Isobe, H. C. Cho, and J. E. Crowell, *Surf. Sci.* **295**, 99 (1993).
- ¹⁶B. Voigtlander, T. Weber, P. Smilauer, and D. E. Wolf, *Phys. Rev. Lett.* **78**, 2164 (1997).
- ¹⁷Y.-W. Mo and M. G. Lagally, *J. Cryst. Growth* **111**, 876 (1991); Y.-W. Mo, R. Kariotis, B. S. Swartzentruber, M. B. Webb, and M. G. Lagally, *J. Vac. Sci. Technol. A* **8**, 201 (1990).
- ¹⁸A. J. Hoven, D. Dijkkamp, E. J. van Loenen, J. M. Lenssinck, and J. Dieleman, *J. Vac. Sci. Technol. A* **8**, 207 (1990).
- ¹⁹R. T. Tung and F. Schrey, *Phys. Rev. Lett.* **63**, 1277 (1989).
- ²⁰J. J. Boland, *Phys. Rev. Lett.* **65**, 3325 (1990).
- ²¹J. E. Vasek, Z. Zhang, C. T. Salling, and M. G. Lagally, *Phys. Rev. B* **51**, 17 207 (1995).